J Mater Sci (2011) 46:2422–2430
DOI 10.1007/s10853-010-5088-x

# Effect of the microstructure on the intercalation and exfoliation behaviour of graphite

**Olga Khvostikova · Helmut Hermann · Horst Wendrock · Thomas Gemming · Jürgen Thomas · Helmut Ehrenberg**

Received: 3 May 2010 / Accepted: 16 November 2010 / Published online: 3 December 2010


**Abstract** The process of the preparation of graphitic nanoplatelets via chemical intercalation and thermal exfoliation of graphite was considered. The dependence of the properties of the final product on the microstructure of the raw material and on different process parameters was analyzed. It is shown that the microstructure of the raw material has considerable influence on the structural transformations during the different preparation steps. The observed differences can be understood assuming that intercalation is initiated at the edges of graphite crystallites by the formation of intercalate nuclei. Essential differences of the nucleation time appear for unequal types of microstructure and give rise to different intercalation states. It is also shown that the sub-process of washing and drying the samples after intercalation is most critical and has significant influence on the characteristics of the final products. The results suggest that graphite fibres with sub-micron diameter and orientation of the crystallographic *c*-axis along the fibre axis will be particularly favourable for the preparation of graphitic nanoplatelets.

## Introduction

Exfoliated graphite is a porous material with numerous well-known applications, e.g. gaskets, sealings, fire extinguisher agents, thermal insulators, conductive resin composites, adsorbents for materials with large molecular size, etc. [1, 2]. Recently, possible applications like electrodes for lithium ion batteries [3–5], supercapacitors [6, 7], and inexpensive filler substitute for carbon nanocomposites [8–11] have been considered. Although exfoliation of graphite was discovered already in 1891 [12, 13] the study and improvement of methods for the preparation of conventional exfoliated graphite, graphitic nanoplatelets, and single-layer graphene sheets is subject of actual research [1, 2, 14–23].

It is an important challenge to develop preparation methods which will be amenable to large-scale production of graphene. Exfoliation of graphite is one of the promising ways to reach this target. Various methods of intercalation and exfoliation of graphite have been developed [1, 14–23]. While most of the corresponding scientific work has been devoted to the preparation methods only few work has been done regarding the effect of the microstructure of different starting material on the properties of the exfoliated materials. The latter point is, however, important. In [18], it was shown that the size of graphite flakes used for exfoliation has considerable impact on porosity, specific surface area, exfoliation volume, and density which directly influence the sorption capacity of heavy oil. Therefore, it is interesting to analyse how different carbon species, e.g. graphite flakes with different lateral dimension of well-ordered areas and different thickness, or polycrystalline powder particles, behave under equal preparation conditions. It is important to define the mechanisms of structure formation and to understand which microstructural features of the initial materials are relevant for the preparation process.

It is the object of the present article to study the structure and the properties of chemically prepared sulphuric-acid graphite intercalation compounds (GICs) and to analyze the effect of the microstructure of different raw materials on the behaviour of the materials during the preparation

O. Khvostikova · H. Hermann (✉) · H. Wendrock · T. Gemming · J. Thomas · H. Ehrenberg
IFW Dresden, Institute for Complex Materials, P.O. Box 27 01 16, 01171 Dresden, Germany
e-mail: h.hermann@ifw-dresden.de

processes and on the parameters of the final exfoliated products. The sensitivity of preparation processes to changes of the microstructure is tested for different process parameters such as temperature and length of process time. It is shown that the intercalation process is controlled by nucleation of intercalate molecules at the edges of graphite crystallites and subsequent diffusion into the graphite crystallite.

## Experimental

### Sample preparation

The following raw materials were used: (i) Natural graphite flakes, type Madagaskar, with nominal purity of 99.9% (NSG Naturgraphit GmbH). Small and big flakes were separated from the material by sieving. The linear dimension in *c*-direction (thickness) was about 50 μm for small and 100 to 200 μm for big flakes. The lateral size was 100 to 500 μm and 500 to 800 μm for small and big flakes, respectively. (ii) Spectral carbon-graphite with nominal purity of 99.999% (SGL Carbon Ringsdorf) with broad particle size distribution ranging from 1 to 100 μm). (iii) Highly oriented pyrolytic graphite (HOPG) samples with size of 10 × 10 × 1 $mm^3$ and nominal impurity level of 10 ppm ash or better (SPI-2 grade, SPI Supplies/Structure Probe, Inc.).

The samples were chemically intercalated following the method described in [16]. The graphite particles were immersed in a mixture of concentrated $H_2SO_4$ (96%) and $HNO_3$ (65%) with a volume ratio of 3:1 and mixed by shaking. The intercalation process was supported by stirring of the samples for different times from 15 min to 8 h at temperatures from 25 to 80 °C. Afterwards, the intercalated materials were washed with distilled water and air-dried. The drying process was carried out for 24 h at the temperature of 100 °C. Finally, the exfoliation process was executed by heating the samples at 1,000 °C in vacuum.

### Sample characterization

X-ray diffraction (XRD) techniques were used to characterize the structure and the structural changes of the samples due to the intercalation process. The families of (hk0) and (00l) reflections were collected separately using, respectively, transmission XRD (Mo-Kα radiation, STOE & Cie.) and reflection XRD (Co-Kα, Philips X′Pert). The lattice parameter c and the stacking sequence of the intercalated layers were evaluated from the (00l) reflections, and the changes of the in-plane structure of the layers were determined from the positions of the reflections (hk0) [24]. The number, *n*, of regularly ordered graphene planes separating two parallel intercalation layers is called the stage number.

In the present case of sulphuric-acid GICs, $HSO_4^-$ ions are intercalated together with $H_2SO_4$molecules, and a stage I GIC is represented as $C_{24}HSO_4{\cdot}2.5H_2SO_4$ [25]. For $n = 1, 2, 3,\ldots$, the chemical composition is approximated by the formula $C_{8n}H_2SO_4$ [26, 27]. The distance of two graphene planes separated by a sulphuric-acid interlayer is $d_s = 7.98$ Å while the graphene–graphene distance in pure graphite is $c_0 = 3.35$ Å. Figure 1 illustrates the arrangement of a sulphuric-acid ion between two graphene layers and Fig. 2 shows different microstructural variants of intercalated graphite.

Denoting the diffraction intensity generated by stage *n* and the entire intensity of a sample by $I_n$ and *I*, respectively, the ratio $R_n$

$$R_n = \int I_n(q)\mathrm{d}q \Big/ \int I(q)\mathrm{d}q$$

was used as a measure for the fraction of material with stage *n* in the sample.

The morphology of the particles was investigated by scanning electron microscopy (SEM) using a Gemini 1530 (Zeiss). EDX measurements (Gemini 1530) were carried out to evaluate the chemical composition and the spatial

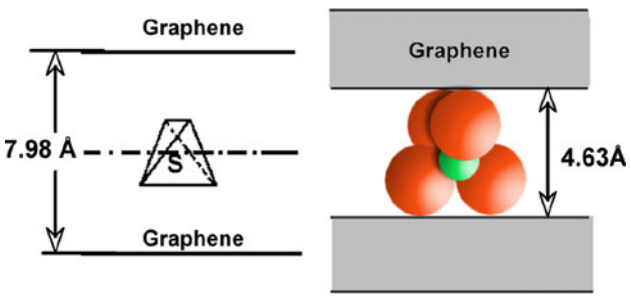


**Fig. 1** Sulphuric-acid ion between two graphene layers

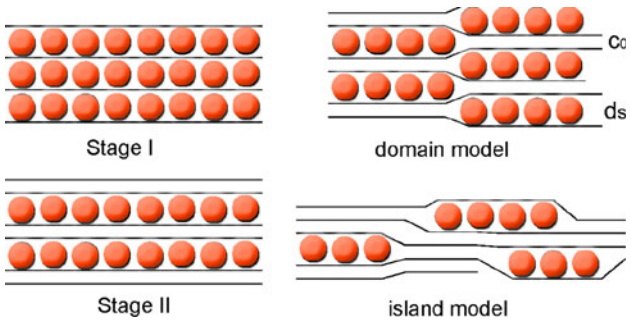


**Fig. 2** Structure of graphite intercalation compounds; *bold lines* cross sections of graphene planes, *circles* intercalated layer, $c_0$ interlayer distance of graphite, $d_s$ distance of two graphene planes separated by an intercalation layer; ordered stages 1 and 2 (*left*), domain model for stage 2 (*top right*), and island model (*down right*)

distribution of the intercalate elements. TEM experiments were performed with a FEI Tecnai F30 microscope operated at 300 kV.

## Results

### Starting material

The elemental composition of powder and flake materials was tested using EDX. The composition was measured at four different test areas each about $50 \times 50$ μm$^2$. The results in at% for flakes (powder) are: 98.12 (99.52) C, 1.09 (0.06) Al, 0.28 (0.01) Si, 0.01 (0.03) P, 0.05 (0.16) S and 0.45 (0.22) Na. The relative statistical errors calculated from the fluctuations of the data are 2 and 3% for the flakes and the powder material, respectively. The purity of the HOPG samples of 10 ppm ash or better was certified by the producer (www.2spi.com/catalog/new/hopgsub.php). Images of the starting materials are shown in Fig. 3.

Rietveld refinement on the XRD patterns was carried to determine the mean size of coherently scattering crystalline areas. The model of cylindrically shaped particles was assumed where the cylinder axis was chosen in the crystallographic $c$-direction. The thickness in $c$-direction and the cylinder diameter are denoted by $h_c$, and $d_{hk}$, respectively. The results are: $h_c = 20$–$50$ nm, $d_{hk} = 80$–$150$ nm for the powder and $h_c > 200$ nm, $d_{hk} > 500$ nm for both types of flakes. Both correlation lengths of HOPG are larger than the spatial resolution of about 500 nm achieved by XRD. The results for the graphene planes distance are $c_0 = 3.35 \pm 0.01$ Å for flakes and HOPG, and $c_0 = 3.36 \pm 0.02$ Å for powder. The lateral grain size of the HOPG samples was of the order of 500 μm and the mosaic angles were $0.8° \pm 0.2°$ (www.2spi.com/catalog/new/hopgsub.php).

The morphology of the flakes (Fig. 3b) shows that the single flakes are either single crystals or mosaic crystals with minimum grain size as determined by the Rietveld analysis. The powder particles appear as randomly shaped porous polycrystals (Fig. 3c) where the lateral size of the crystallites is of the order of 1 μm and their thickness is on the 0.1 μm scale (Fig. 3d). This corresponds to the results of the Rietveld analysis. The orientation of the crystallites within the powder particles is predominantly random on the sub-μm scale (Fig. 3d).

### Intercalation

All samples changed their colour from dark gray to blue during the intercalation process. This well-known transition [28, 29] indicates the formation of intercalation states with low stage numbers. The details of this transition differed for the diverse raw materials and varied also with changing process temperatures. The results are collected in Table 1.

At ambient temperature (25 °C), the graphite flakes turned from gray to blue after short shaking, the graphite

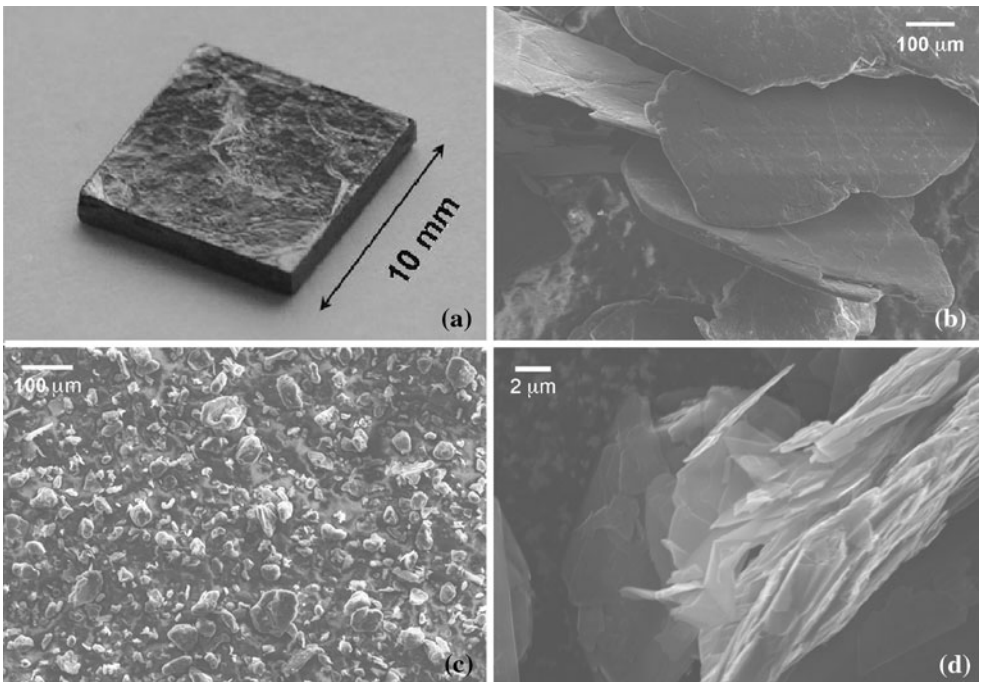


**Fig. 3** Images of samples of the starting materials; HOPG (**a**, optical), graphite flakes (**b**, SEM), and graphite powder (**c**, **d**, SEM)

**Table 1** Properties of intercalated graphitic materials

| Time of stirring | Ambient conditions | | | 50 °C | | 80 °C | | |
|---|---|---|---|---|---|---|---|---|
| | Big flakes | Small flakes | Powder | Big flakes | Small flakes | Big flakes | Small flakes | Powder |
| Short shaking | Blue<br>Stages II + III | Blue<br>Stage II<br>Traces of stage III | Dark grey | Blue colour | Blue colour | Blue<br>Stages II + III | Blue<br>Stage II<br>Traces of III | Dark grey |
| 15 min | Blue<br>Stages II + I<br>$R_I \approx 25\%$ | Blue<br>Stages II + I<br>$R_I \approx 5\%$ | Dark grey | Blue<br>Stages II + I<br>$R_I \approx 25\%$ | Blue<br>Stages II + I<br>$R_I \approx 15\%$ | Blue<br>Stages II + I<br>$R_I \approx 10\%$ | Blue<br>Stages II + I<br>$R_I \approx 20\%$ | Dark grey/Blue |
| 30 min | Blue<br>Stages II + I<br>$R_I \approx 25\%$ | Blue<br>Stages II + I<br>$R_I \approx 20\%$ | Dark grey/Blue | Blue<br>Stages II + I<br>$R_I \approx 30\%$ | Blue<br>Stages II + I<br>$R_I \approx 20\%$ | Blue<br>Stages II + I<br>$R_I \approx 15\%$ | Stage II | Blue |
| 1 h | Blue<br>Stages II + I<br>$R_I \approx 25\%$ | Blue<br>Stages II + I<br>$R_I \approx 20\%$ | Blue | Blue<br>Stages II + I | Blue<br>Stages II + I<br>$R_I \approx 15\%$ | Blue<br>Stages II + I<br>$R_I \approx 15\%$ | Blue<br>Stage II | Blue |
| 2 h | Blue<br>Stages II + I<br>$R_I \approx 25\%$ | Blue<br>Stages II + I<br>$R_I \approx 15\%$ | Blue<br>Stages II + I<br>$R_I \approx 50\%$ | Blue<br>Stages II + I<br>$R_I \approx 30\%$ | Blue<br>Stages II + I<br>$R_I \approx 15\%$ | Blue<br>Stages II + I<br>$R_I \approx 20\%$ | Blue<br>Stage II | Blue<br>Stage II |
| 4 h | Blue<br>Stages II + I<br>$R_I \approx 20\%$ | Blue<br>Stages II + I<br>$R_I \approx 20\%$ | Blue<br>Stages II + I<br>$R_I \approx 50\%$ | Blue<br>Stages II + I<br>$R_I \approx 30\%$ | Blue<br>Stages II + I<br>$R_I \approx 15\%$ | Blue<br>Stages II + I<br>$R_I \approx 15\%$ | Blue<br>Stages II + III | Blue<br>Stage II |
| 6 h | Blue<br>Stages II + I<br>$R_I \approx 40\%$ | Blue<br>Stages II + I<br>$R_I \approx 15\%$ | Blue<br>Stages II + I | Blue<br>Stages II + I<br>$R_I \approx 40\%$ | Blue<br>Stages II + I<br>$R_I \approx 20\%$ | Blue<br>Stages II + I<br>$R_I \approx 10\%$ | Blue<br>Stages II + I | Blue<br>Stage II |
| 8 h | Blue<br>Stages II + I<br>$R_I \approx 40\%$ | Blue<br>Stages II + I<br>$R_I \approx 20\%$ | Blue<br>Stages II + I<br>$R_I \approx 70\%$ | Blue<br>Stages II + I<br>$R_I \approx 40\%$ | Blue<br>Stages II + I<br>$R_I \approx 15\%$ | Blue<br>Stages II + I<br>$R_I \approx 15\%$ | Blue<br>Stage II | Blue<br>Stage II |

powder remained dark gray until 15 min of stirring and changed completely from gray to blue colour after 1 h. The surface of HOPG platelets turned also from gray to blue after short shaking, but the inner part of the samples stayed dark gray. Size and shape of the samples did not change after the process of short shaking.

After some time of stirring an increase of the thickness of the flake-like samples and of the HOPG platelets in the direction of the *c*-axis was visible. The shape of the samples was, however, maintained.

XRD measurements and the determination of the intensity ratio $R_n$ gave quantitative results for the formation of the intercalation states. Figure 4 shows diffraction patterns for big-flake samples taken after different process steps.

For the flake-like samples, mixtures of stages II and III were observed during the intercalation process already after short shaking, and the stages I and II appeared after 15 min of stirring. Values of $R_I$ of 20 and 40% were achieved for, respectively, small and big flakes after 8 h of stirring. The highest value for $R_I$ was obtained with the powder sample and reached 70% after 8 h of stirring.

The sensitivity of the intercalation process with respect to the temperature was tested by repeating the experiment at 50 °C (small and big flakes) and 80 °C (small flakes, big flakes, powder). No essential difference was observed between the results for 25 and 50 °C.

At the temperature of 80 °C, stage I was not observed for graphite powder over the complete course of the process. The value $R_I = 15\%$ obtained at 80 °C for the big flakes was much smaller than that observed at 25 °C. Additionally, there was no indication of stage I for small flakes and for graphite powder even after 8 h of stirring. As a result, we conclude that enhanced reaction temperatures do not favour the formation of stage I. The formation of the intercalation states with stages I and II and the fraction of stage I is quite different for the flake-like samples and the powder material. This will be discussed later.

In order to test whether or not the material has reached a stationary state after 8 h of stirring all samples were left in

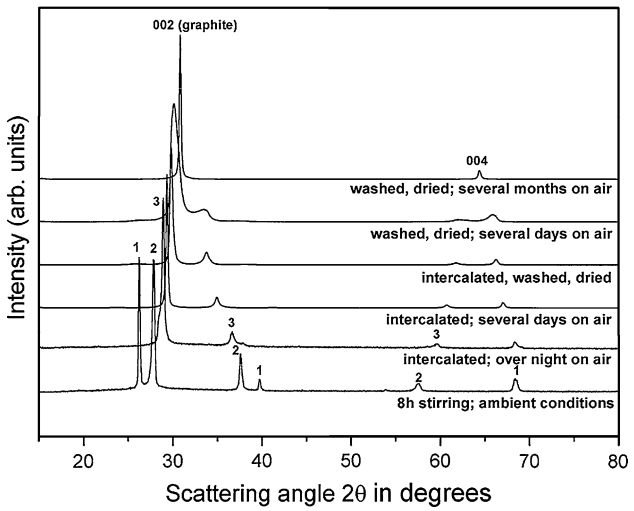


**Fig. 4** XRD patterns (reflection geometry, Co-Kα radiation) of graphite sulphates obtained for big-flake samples after different process steps (Numbers *1*, *2*, *3* indicate the stage number responsible for the corresponding reflections.)

closed chambers at the intercalation temperature for an additional period of one day. XRD patterns of the samples stirred in the mixture of acids for 8 h and the patterns obtained from the materials left in the chambers for longer time indicated no difference. This means that the state achieved after 8 h can be considered as a stationary one.

## Washing and drying

After washing and drying the graphite-flake and HOPG samples showed a textured microstructure with stacked graphitic sheets. The graphite powder samples appeared as random microstructures resembling the shape of heads of lettuce. The largest dimension regarding the thickness of the graphite sheets separated after washing and drying was about 1 μm for all samples. The different morphologies are illustrated in Fig. 5.

According to EDX measurements the sulphur was mostly concentrated in regions of folded layers and between separated graphite sheets. The average concentration of sulphur was about 5 at% for all samples.

The nanostructure of the materials changed dramatically during washing and drying. The materials lost the low-stage states. XRD patterns for flake-like materials showed broad diffraction peaks pointing to stage numbers of V to VIII. The material was transformed from the ordered state into a disordered graphitic structure including clusters of intercalate molecules. This resembles the island-like structure model of residue compounds [30]. For the HOPG samples the structure was identified as a mixture of stages III and IV. Graphite powder showed no staging at all after washing and drying.

It was also discussed in [14] that hydration of the intercalated material is responsible for the degradation of the ordered intercalation state. Here, the hydration process was traced by subjecting the sample to air moisture. The XRD diagrams shown in Fig. 4 illustrate the degradation process due to hydration. The sample (big flakes) was characterized by a mixture of stages I and II immediately after 8 h intercalation process. The stages I and II disappeared after 12 h of exposure to air moisture and stage III was detected. The XRD diagram taken after several days of exposure to air moisture approached that obtained from the corresponding sample after washing and drying. Finally, the hydration process resulted in a state characterized by the (002) and (004) reflections of pure graphite. The XRD results were confirmed by qualitative visual inspection of the samples which showed the transition from blue colour to gray in the course of the hydration process.

## Exfoliation

As a result of the exfoliation process, neighbouring graphite layers were separated due to the pressure of the evaporating species and systems of loosely packed graphitic platelets were formed. It is obvious that the

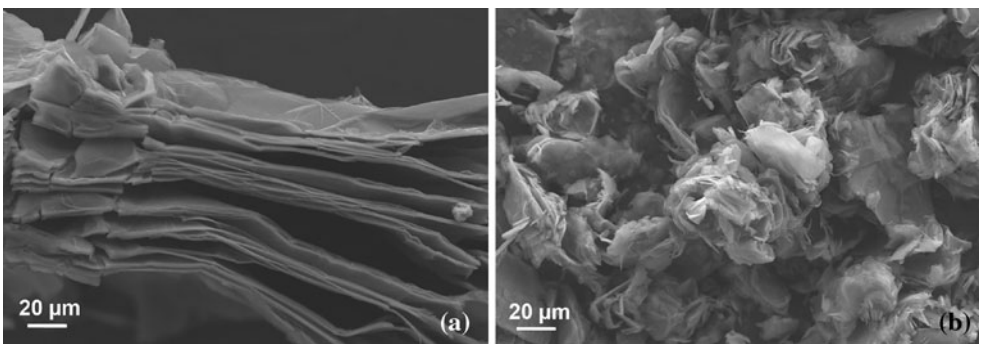


**Fig. 5** Morphology of small graphite flakes (**a**), and graphite powder (**b**) after intercalation, washing and drying

geometric distribution of the intercalated species determines how the material is exfoliated. This concerns especially the thickness of the graphite platelets and the character and the degree of porosity of the exfoliated material. For example, the exfoliation of a GIC with stage number III is expected to result in a porous material with pore walls consisting of three stacked graphene layers.

The process of exfoliation run very rapidly and took place simultaneously in all intercalated parts of the material. The structure of the graphite sulphates was completely destroyed after exfoliation. The XRD patterns indicated only reflections of pure graphite. Preferred orientations present in the initial states of both flake-like materials and HOPG-samples were eliminated after exfoliation. The EDX measurements revealed that the content of sulphur after heat treatment was less than 1 at% for all materials. The morphology of the exfoliated samples on the micrometre scale is illustrated in Fig. 6. The samples prepared from big flakes turned to long worm-like particles (Fig. 6a), and the small flakes exfoliated to puffed-up sponge-like particles of different size (Fig. 6b). Both flake-like samples were characterized by crinkled surfaces of the graphitic sheets and random morphology where the separated graphite platelets were, on average, thinner for the small-flake samples than for the big-flake ones.

The exfoliated powder samples (Fig. 6c) showed a comparatively low increase of the volume. The microstructure resembled the morphology of lettuce heads. The exfoliated sheets were also randomly distributed but were not as rigorously crumpled as in the case of the flake-like samples. The morphology of the exfoliated HOPG samples is illustrated in Fig. 6d. The particles are worm-like as in the case of the flake-like samples. The enlargement of the volume of the exfoliated HOPG samples was between that of the flake-like samples and the powder material. Some HOPG samples were cut into pieces of about $3 \times 3 \times 1$ mm$^3$. This material showed an exfoliation behaviour which was very similar to that of big flakes but with significantly smaller exfoliation volume.

Figure 7 illustrates the microstructure of exfoliated flake-like samples on the scale of 10 nm to 1 μm. The SEM images show crumpled and folded graphitic sheets with values of the thickness between 10 and 100 nm where the lower value is close to the resolution of the microscope. Considerable fractions of thin sheets with about 10 nm thickness were observed for the flake-like samples where the fraction of such sheets was significantly higher for the small-flake samples than for the big-flake ones. Sheets with a thickness of few tens of nanometres were observed for exfoliated HOPG samples, and the values for the powder samples were of the order of 100 nm.

The SEM images revealed qualitatively, that the fraction of platelets with a thickness of the order of 10 nm is much higher for the small-flake samples than for all other investigated materials.

TEM investigations were carried out for all types of exfoliated samples. Figure 8 shows an image obtained from an exfoliated small-flake sample. Thin graphitic

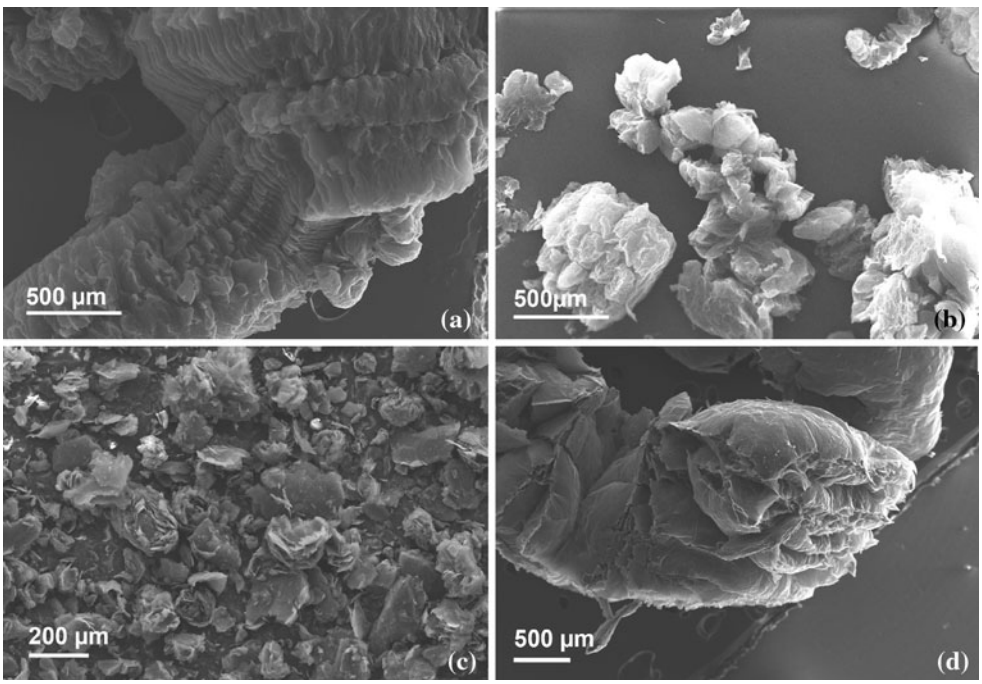


**Fig. 6** Morphology of exfoliated samples; **a** big flakes, **b** small flakes, **c** graphite powder, **d** cut HOPG sample

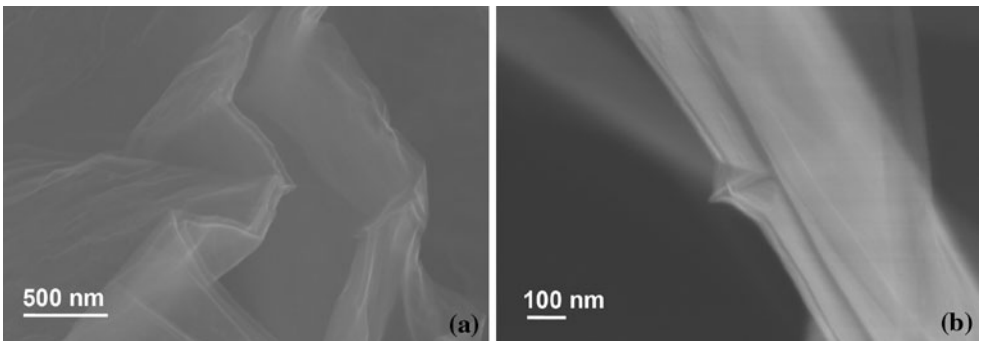


**Fig. 7** Morphology of graphitic sheets of exfoliated graphite; **a** big flakes, **b** small flakes

sheets composed of 12 stacked graphene layers are visible. The fraction of graphitic sheets with a thickness in the range between 2 and 5 nm could not be quantified. However, it appeared qualitatively that the fraction of sheets with a thickness below 5 nm was higher for small-flake samples than for all other ones.

XRD patterns were taken from each type of exfoliated samples. In order to estimate the degree of inhomogeneity of the samples, 5 different specimens of each sample type were analyzed. Figure 9 shows typical XRD patterns. The cylindrical shape model was used for the Rietveld analyses to determine thickness, $h_c$, and lateral size (or correlation length of the crystalline order), $d_{hk}$, of the graphene platelets, and the lattice constant, $c$. The result for the $c$-values is $c = 3.35 \pm 0.02$ Å and does not depend on the sample type. For the powder sample, $h_c = 15$–$20$ nm and $d_{hk} \approx 10$ nm was obtained. The values of exfoliated HOPG samples and flake-like materials are $h_c = 5$–$30$ nm and $h_c = 5$–$10$ nm, respectively, and the lateral correlation length is about $d_{hk} \approx 10$ nm. This is illustrated by TEM observations shown in Fig. 8 where graphene platelets with thickness of 5 nm are visible. The TEM image shows also that the lateral size of the platelets is larger than the correlation length of crystalline order which is disturbed by dislocations and the curvature of the platelets.

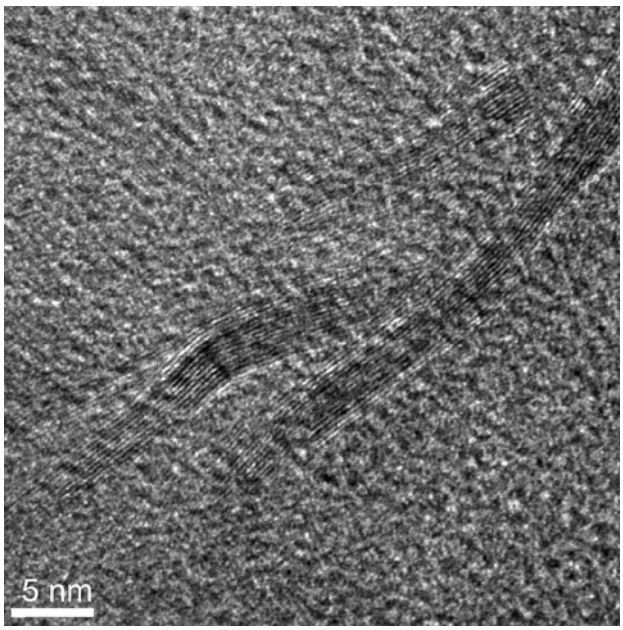


**Fig. 8** TEM image of thin graphitic sheets observed for small flakes after exfoliation

## Discussion

The intercalation process proceeded differently for the different starting materials. After immersion of the samples in the $H_2SO_4/HNO_3$ mixture a delay time was observed until the onset of significant formation of stages I and II. This delay time was about 15 min, 30 min, and 2 h for big-flake, small-flake, and powder samples, i.e. the delay time was long for small thickness of crystallites, and vice versa. Despite their long delay time the powder samples showed the highest fraction of stages I and II after 8 h of stirring. Increasing the process temperature from ambient temperatures to 50 °C improves the yield of stages I and II only slightly, and the fraction of stage I material obtained at 80 °C was significantly smaller than that achieved at lower temperatures. Stage II was obtained at all temperatures after a sufficiently long period of stirring which suggests the assumption that stage II is the most stable intercalation state under the experimental conditions applied here.

The dissimilar intercalation behaviour of the different samples could be caused either by chemical impurities or by the morphology of the particles. Chemical impurities can be excluded as reason for the different behaviour of small and big flakes because the impurity content is identical in both samples. Additionally, the fraction of impurities is very small for all samples so that it seems implausible to take this into account as reason for the dissimilar intercalation behaviour. Instead, the unequal morphologies of the particles of the different samples have to be considered.

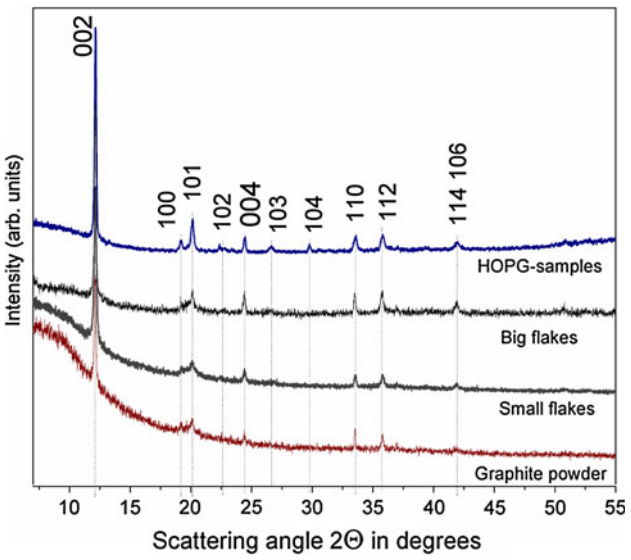


**Fig. 9** XRD patterns of exfoliated samples (The different background scattering was caused by glue used for sample preparation.)

It is known from intercalation in the gas phase that the process of intercalation is initiated at the edges of the graphite crystal (see [30] and references therein). This activation process retards the diffusion into the bulk material since the activation energy for the formation of intercalate nuclei at the graphite crystal edges is higher than the activation energy for the diffusion of the intercalate molecules along the graphene layers. Figure 10 illustrates the formation of an intercalate nucleus at the edge of a graphite crystal and the diffusion of intercalate molecules from this nucleus into the graphene layer structure.

The diffusion constant of nitric acid in graphite is $D = 2 \times 10^{-6}$ cm$^2$/min [31]. Assuming the same value for sulphuric acid the diffusion time $t = R^2/D$ required to intercalate a given particle can be estimated. For small flakes (50 μm $\leq R \leq$ 250 μm) and big flakes (250 μm $\leq R \leq$ 400 μm) one obtains 0.1 to 3 min and 3 to 8 min, respectively. Considering that after 15 min only 5 and 25% volume fraction of the small and big flakes, respectively, were intercalated it follows that the diffusion process can not be the limiting factor for the intercalation process. This applies also to the powder sample.

On the other hand, the thickness of big flakes (100 to 200 μm), small flakes (about 50 μm), and the crystallites in the powder particles (between few tens of nanometres observed by Rietveld analysis and about 0.1 μm by SEM, Fig. 3d) can be related to the kinetics of the intercalation. Clearly, decreasing thickness of the graphite crystallites correlates with increasing delay time for stage I and II formation (Table 1). This conclusion is consistent with the observations for intercalation from the gas phase [30].

The final fraction of stage I and II in the powder samples is, however, very high (70%) compared to 20 and 40% for small and big flakes, respectively. This can be understood in terms of the strain model for the intercalation process which proposes that thin samples intercalate more readily than thick ones because of the lower elastic impedance of thin samples [30].

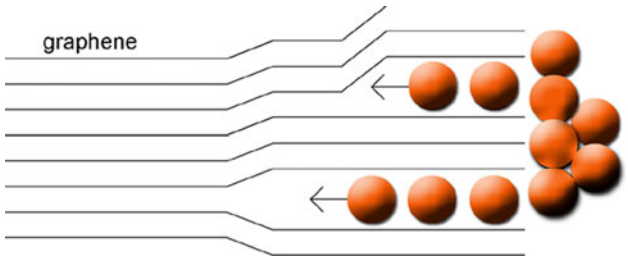


**Fig. 10** Nucleation of intercalate molecules at the edge of a graphite crystal and intercalation by diffusion

The present experimental conditions required to remove residual acid from the samples after intercalation. This was done by washing and drying the GICs. The process of washing and drying had, however, dramatic effect on the structure. The powder material showed no distinct staging after washing and drying. However, mixtures of stages V to VIII and III and IV were observed by XRD for flake-like material and HOPG samples, respectively, after washing and drying. Clearly, the smaller the size of graphite crystallites the more dramatic is the destruction of the intercalation state of the samples.

The time evolution of the hydration process was observed by exposure of intercalated big-flake samples to air moisture. The initial state described by stages I and II (Fig. 4) changed to pure stage III after 12 h and transformed finally to well-ordered graphite without any indication of staging.

Obviously, the process step of washing and drying shows a considerable potential of optimizing the preparation of graphitic platelets with defined thickness on the nanometre-scale.

The exfoliation process lead to different results for the different samples as well. The enlargement of the volume was high and medium for flake-like and powder material, respectively, and it was in between for HOPG. For exfoliated small-flake samples much more nanometre-scale graphitic sheets were detected than for the other materials as the high-resolution SEM and TEM observations showed. It should be noted that these fine sheets can be easily separated by immersing the material in ethanol and ultrasound stirring.

## Conclusion

The success of the method of intercalation and exfoliation of graphitic material regarding the preparation of

nanometre-scale graphitic particles depends significantly on the microstructure of the initial material. Correlations of the kinetics and the result of all process steps with the dimension of the graphite crystals and crystallites in *c*-direction and the lateral size were found. From the present observation it can be concluded that cylindrical graphite crystallites with *c*-axis in the direction of the cylinder axis would be most favourable for the preparation of graphene nanoplatelets, and single-, double-, or triple-graphene layers which show interesting electronic, thermal, and mechanical properties [32–34]. Graphite fibres with about 200 nm diameter and lengths of few μm, and *c*-axis in the direction of the fibre line will be available soon [35] and will be used as a new starting material.

**Acknowledgements** Financial support by EnBW Energie Baden-Württemberg AG is gratefully acknowledged. This study has also benefited from support from the European Union and the Free State of Saxony within the European Centre for Emerging Materials and Processes Dresden (ECEMP, grant no. 13858/2379).

## References

1. Chung DDL (1987) J Mater Sci 22:4190. doi:10.1007/BF0113
2. Celzard A, Marêché JF, Furdin G (2005) Progr Mater Sci 50:93
3. Konno H, Morishita T, Sato S, Habazaki H, Inagaki M (2005) Carbon 43:1110
4. Konno H, Morishita T, Wan C, Kasashima T, Habazaki H, Inagaki M (2007) Carbon 45:477
5. Zou L, Kang F, Zheng YP, Shen W (2009) Electrochim Acta 54:3930
6. Wan C, Azumi K, Konno H (2007) Electrochim Acta 52:3061
7. Mitra S, Lokesh KS, Sampath S (2008) J Power Sources 185:1544
8. Kalaitzidou K, Fukishima H, Drzal LT (2007) Carbon 45:1445
9. Debelak B, Lafdi K (2007) Carbon 45:1727
10. Ganguli S, Roy AK, Anderson DP (2008) Carbon 46:806
11. Afanasov IM, Morozov VA, Kepman AV, Ionov SG, Seleznev AN, Van Tendeloo G, Avdeev VV (2009) Carbon 47:263
12. Luzi W (1891) GB patent 9922
13. Boehm HP, Stumpp E (2007) Carbon 45:1381
14. Oh WC, Bae NK, Choi YJ, Ko YS (1995) Carbon 33:323
15. Kang F, Zheng YP, Wang HN, Nishi Y, Inagaki M (2002) Carbon 40:1575
16. Inagaki M, Tashiro R, Washino Y, Toyoda M (2004) J Phys Chem Solids 65:133
17. Tryba B, Morawski AW, Inagaki M (2005) Carbon 43:2417
18. Vieira F, Cisneros I, Rosa NG, Trindade GM, Mohallem NDS (2006) Carbon 44:2590
19. Stankovich S, Piner RD, Chen X, Wu N, Nguyen ST, Ruoff RS (2006) J Mater Chem 16:155
20. Stankovich S, Dikin DA, Piner RD, Kohlhaas KA, Kleinhammes A, Jia Y, Wu Y, Nguyen ST, Ruoff RS (2007) Carbon 45:1558
21. Li J, Liu Q, Da H (2007) Mater Lett 61:1832
22. Osváth Z, Darabont A, Nemes-Incze P, Horváth E, Horváth ZE, Biró LP (2007) Carbon 45:3022
23. Wei T, Fan Z, Luo G, Zheng C, Xie D (2009) Carbon 47:337
24. Hérold A (1979) In: Levy F (ed) Intercalated layered materials, vol 6. D Reidel Publishing Company, Dordrecht, p 323
25. Shioyama H (2000) Synth Met 114:1
26. Rüdorff W, Hoffmann U (1938) Z Anorg Allgem Chem 238:1
27. Rüdorff W (1940) Z Phys Chem B 45:42
28. Brodie BC (1845) Annales de chimie et de physique 45:351
29. Wiberg N (2007) Holleman-Wiberg Lehrbuch der Anorganischen Chemie. Walter de Gruyter, Berlin
30. Dresselhaus MS, Dresselhaus G (2002) Adv Phys 51:1
31. Dowell MB, Badorrek DS (1978) Carbon 16:241
32. Novoselov KS, Geim AK, Morozov SV, Jiang D, Zhang Y, Dubonos SV, Grigorieva IV, Firsov AA (2004) Science 306:666
33. Geim AK, Novoselov KS (2007) Nat Mater 6:183
34. Oostinga JB, Heersche HB, Liu X, Morpurgo AF, Vandersypen LMK (2008) Nat Mater 7:151
35. Ritschel M, Leonhardt A, Helbig J, Knöchel D (2010) In: Proceedings of the 8th Int. Nanotechnology Symposium, Dresden, July 6–7, 2010